Non-linear acoustic properties and acoustic-mode vibrational anharmonicity of 18R martensite Cu-Zn-Al shape-memory alloy

1998 J. Phys.: Condens. Matter 10 9737

(http://iopscience.iop.org/0953-8984/10/43/017)

J. Phys.: Condens. Matter **10** (1998) 9737–9746. Printed in the UK PII: S0953-8984(98)95464-9

Non-linear acoustic properties and acoustic-mode vibrational anharmonicity of 18R martensite Cu–Zn–Al shape-memory alloy

Alfons Gonzàlez-Comas†, Lluís Mañosa†, M Cankurtaran‡‖, G A Saunders‡ and F C Lovey§

† Departament d'Estructura i Constituents de la Matèria, Universitat de Barcelona, Diagonal 647, Facultat de Física, E-08028 Barcelona, Catalonia, Spain

‡ School of Physics, University of Bath, Bath BA2 7AY, UK

§ Centro Atómico de Bariloche, 8400, San Carlos de Bariloche, Argentina

Received 1 July 1998

Abstract. To shed further light on the dynamics of the martensitic transformation in shape-memory alloys, measurements have been made of the effects of hydrostatic pressure on the velocities of 15 different pure ultrasonic modes propagated at room temperature in a $Cu_{0.696}Zn_{0.128}Al_{0.176}$ single-crystal alloy in its 18R martensitic phase. Although the point symmetry group of the 18R martensite is monoclinic, the elastic behaviour can be reasonably described in terms of an orthorhombic structure; the further monoclinicity beyond such an orthorhombic representation is very small and can be neglected to a first approximation. The results obtained for the nine independent second-order elastic stiffness tensor components C_{IJ} in the 18R structure and their hydrostatic-pressure derivatives $(\partial C_{IJ}/\partial P)_{P=0}$ have been used to calculate the mode Grüneisen parameters $\gamma_p(N)$, which quantify the vibrational anharmonicity of long-wavelength acoustic phonons. Results are compared with those computed from TOEC data measured on a β-phase Cu–Zn–Al single crystal with a similar composition. At room temperature, about 28 K below the martensitic transition temperature (=323 K), the longitudinal mode $\gamma_p(N)$ have normal, positive values; however, those $\gamma_p(N)$ associated with some shear modes have negative values. A pronounced minimum has been found in the Grüneisen parameter of the shear mode propagated along the [111] direction with $[1\bar{2}1]$ polarization vector. It is concluded that the lattice stability against this particular shear mode decreases as the sample approaches the martensitic transition.

1. Introduction

Noble-metal-based alloys with a bcc structure (β-phase) can undergo a structural transition to a close-packed phase by a martensitic transformation (MT), which can be induced either by change of temperature or application of pressure. This is a first-order, diffusionless, structural phase transition, which involves a homogeneous shear of the parent bcc phase [1]. Martensitic transformation is the underlying mechanism responsible for many of the unusual thermomechanical properties of these alloys including superelasticity, high damping and the shape-memory effect [2]. Fundamental interest and novel technological applications of these effects have prompted numerous theoretical and experimental investigations of materials that undergo MT, including the Cu-based alloys. Here we focus on Cu–Zn–Al, a typical shape memory alloy.

‖ Permanent address: Hacettepe University, Department of Physics, Beytepe, 06532 Ankara, Turkey.

0953-8984/98/439737+10$19.50

When bcc solids approach a martensitic transformation, a number of precursor phenomena intimately related to the transformation mechanism can occur. These alloys usually exhibit a low $TA_2[110]$ phonon branch, which is accompanied by a low value of the elastic constant C' $(=(C_{11} - C_{12})/2)$. As the material approaches the transition, both the TA_2 phonons and C' soften but not completely: neither phonon frequencies nor elastic constant reach zero at the transition point [3]. Hence, to understand the dynamical behaviour associated with such transitions, it is necessary to go beyond the harmonic approximation and to quantify the vibrational anharmonicity of phonon modes near the martensitic transition temperature (M_s) [4, 5].

Depending on alloy composition, the martensitic transformation takes the high-temperature phase into different crystallographic structures based on different stacking sequences of close-packed planes along the *c*-axis direction. The usual nomenclature uses rhombohedral (R) or hexagonal (H) for the close-packed plane stacking, with a number added which characterizes the number of stacking sequences in the repeat unit. The 18R martensite structure for the alloy studied here is monoclinic [6]. However, for practical convenience, a larger unit cell containing 18 close-packed atomic planes (M18R structure) is used [7]. In the first determination of the elastic stiffnesses of this alloy in terms of a monoclinic structure it was shown that C_{15}, C_{25}, C_{35} and C_{46} were so small that they could be considered to be zero. For this reason it is considered adequate to make pressure dependence measurements of the set of independent elastic stiffness tensor components which correspond to the orthorhombic structure. The Miller indices and the elastic stiffness tensor components and their pressure derivatives throughout refer to the orthorhombic M18R unit cell.

Experimental data which can be used to provide information about the vibrational anharmonicity are available for a number of Cu-based alloys in the bcc phase. By measuring the effects of uniaxial stress on the velocity of ultrasonic modes complete sets of third-order elastic constants (TOECs) have been obtained for several alloys: Cu–Zn–Al [8], Cu–Al–Ni [9] and Cu–Al–Pd [10]. The hydrostatic pressure derivatives have been also determined for Cu–Al–Be [11]. Yet, in spite of the considerable effort made in quantifying the vibrational behaviour on the β-phase, very few measurements have been performed on the corresponding martensite phase. Rodríguez *et al* [12] measured the room-temperature second-order elastic stiffness tensor components (C_{IJ}) of an 18R martensite Cu–Zn–Al alloy single crystal. More recently, some of the present authors measured the temperature dependence of the complete set of elastic stiffness tensor components of the same sample [13]. The main objective of the present work is to provide detailed information about the anharmonicity of long-wavelength acoustic modes of the same Cu–Zn–Al alloy sample studied previously [12, 13] just below its transition temperature to the bcc phase and establish further knowledge of the transition mechanism. To achieve this aim, the hydrostatic pressure derivatives $(\partial C_{IJ}/\partial P)_{P=0}$ of the second-order elastic constants have been determined ultrasonically and are used to obtain the Grüneisen parameters of the acoustic modes in the long-wavelength limit. The anharmonicity of these modes is then compared with those computed from TOEC data measured on a β-phase Cu–Zn–Al single crystal with similar composition [8].

2. Experimental details and techniques

The sample was a martensite Cu–Zn–Al single crystal of composition $Cu_{0.696}Zn_{0.128}Al_{0.176}$, which had been investigated previously by ultrasonic and calorimetric techniques. The alloy of this composition transforms thermoelastically from the β-bcc phase to a monoclinic 18R

martensite structure on cooling below its transition temperature $M_s = 323$ K. For details of sample preparation see Rodríguez *et al* [12]. Large single crystals are required for precision measurements of ultrasonic wave velocities and their pressure dependences. Two cubic-shaped specimens have been studied here: the first one ($9.90 \times 4.15 \times 5.95$ mm^3) with faces parallel to the (100), (010) and (001) planes, the second one ($3.87 \times 5.05 \times 4.53$ mm^3) with two faces parallel to the $(3\bar{2}0)$ and $(\bar{1}\bar{2}8)$ planes.

Ultrasonic wave transit times were measured using the pulse-echo overlap technique [14], capable of resolution of velocity changes to 1 part in 10^5 and particularly well suited to the determination of pressure-induced changes in velocity. X-cut and Y-cut quartz transducers were used to generate and detect longitudinal and shear 10 MHz ultrasonic pulses respectively. Dow Resin 276-V9 was chosen as the bonding material between the specimen and the transducer. Hydrostatic pressures up to 0.15 GPa were applied using a piston and cylinder apparatus with silicone oil as the pressure transmitting medium. The pressure was measured using the change in resistance of a precalibrated manganin wire coil inside the cell. During pressure runs it was important to ensure that measurements were made at the same controlled temperature ($\pm 0.1\,^{\circ}$C) because the ultrasonic wave velocity is sensitive to temperature.

Pressure-induced changes in the sample dimensions were taken into account by using the 'natural velocity (W)' technique [15]. For further details of the experimental set-up see Flower and Saunders [16].

3. Experimental results and discussion

3.1. Hydrostatic pressure derivatives of the elastic stiffness tensor components in the martensite phase

The 18R martensite structure can be closely approximated as being orthorhombic; this approach simplifies the description of its elastic properties [12]. To describe the elastic behaviour of an orthorhombic crystal, nine independent second-order elastic constants are needed; in Voigt notation [17] and matrix form these are

$$C_{IJ} = \begin{pmatrix} C_{11} & C_{12} & C_{13} & 0 & 0 & 0 \\ C_{12} & C_{22} & C_{23} & 0 & 0 & 0 \\ C_{13} & C_{23} & C_{33} & 0 & 0 & 0 \\ 0 & 0 & 0 & C_{44} & 0 & 0 \\ 0 & 0 & 0 & 0 & C_{55} & 0 \\ 0 & 0 & 0 & 0 & 0 & C_{66} \end{pmatrix}. \tag{1}$$

These elastic stiffness tensor components (C_{IJ}) in this orthorhombic reference frame have been determined from the measured velocities of the ultrasonic modes listed in table 1 in which the wave vectors $\boldsymbol{N}$ corresponding to the directions of propagation and the components of the polarization vectors $\boldsymbol{U}$ are given for all measured propagation modes. Velocities of modes with numbers between V1 and V9 have been examined on the larger specimen, while the remainder have been measured on the smaller one. To obtain the complete set of elastic stiffness tensor components (C_{IJ}) as best fits to the experimental data measured for the ultrasonic velocities, it was necessary to use a numerical procedure based on the solution of the wave propagation equations for an orthorhombic symmetry. In an anisotropic crystal the velocities of propagation of longitudinal and shear waves along different directions are related to the set of elastic stiffness tensor components (C_{IJ}) by the Christoffel equations [18]. The fact that the number of equations was larger than

Table 1. Experimental results for the ultrasonic velocity V_0, pulse-echo overlap frequency at atmospheric pressure f_o, its hydrostatic pressure derivative $[\partial f/\partial P]_{P=0}$ and the pressure derivative of the elastic stiffnesses $[\partial(\rho V^2)/\partial P]_{P=0}$ for ultrasonic waves propagating with $\boldsymbol{N}$ and $\boldsymbol{U}$ as propagation vector and polarization vector, respectively. Relationships between elastic constants and propagation velocities are given for a number of modes.

Mode	$\boldsymbol{N}$	$\boldsymbol{U}$	$\rho V^2 = C_{IJ}$	V_0 (m s^{-1})	f_o (kHz)	$[\partial f/\partial P]_{P=0}$ (kHz kbar^{-1})	$[\partial(\rho V^2)/\partial P]_{P=0}$
V1	[001]	[001]	C_{33}	5533	464.939 ± 0.152	0.808 ± 0.040	7.122 ± 0.400
V2	[001]	[010]	C_{44}	2653	222.976 ± 0.007	0.256 ± 0.010	1.008 ± 0.048
V3	[001]	[100]	C_{55}	1862	156.460 ± 0.005	0.215 ± 0.005	0.615 ± 0.017
V4	[010]	[010]	C_{22}	4579	551.741 ± 0.134	1.526 ± 0.056	11.906 ± 0.323
V5	[010]	[001]	C_{44}	2836	341.701 ± 0.017	0.457 ± 0.010	2.823 ± 0.036
V6	[010]	[100]	C_{66}	2241	269.977 ± 0.015	0.229 ± 0.003	1.389 ± 0.008
V7	[100]	[100]	C_{11}	4816	243.256 ± 0.035	0.442 ± 0.008	5.253 ± 0.116
V8	[100]	[010]	C_{66}	2519	127.228 ± 0.002	0.112 ± 0.003	0.535 ± 0.023
V9	[100]	[001]	C_{55}	1867	94.306 ± 0.002	0.126 ± 0.003	0.535 ± 0.017
V10	$[3\bar{2}0]$	$[2\bar{1}0]$	[a]	4927	626.929 ± 0.082	1.304 ± 0.010	7.308 ± 0.057
V11	$[3\bar{2}0]$	[231]	[a]	2303	297.503 ± 0.152	0.453 ± 0.006	1.207 ± 0.016
V12	$[3\bar{2}0]$	$[\bar{9}131]$	[a]	1653	227.746 ± 0.037	0.302 ± 0.034	0.565 ± 0.065
V13	$[\bar{1}\bar{2}8]$	$[\bar{9}131]$	[a]	5113	564.380 ± 0.061	1.198 ± 0.019	10.294 ± 0.134
V14	$[\bar{1}\bar{2}8]$	[801]	[a]	2752	303.788 ± 0.008	0.239 ± 0.028	1.446 ± 0.106
V15	$[\bar{1}\bar{2}8]$	$[10\bar{9}\bar{1}]$	[a]	1047	115.591 ± 0.002	0.310 ± 0.005	0.525 ± 0.008

[a] The data for the modes V10–V15 are obtained from third-order algebraic equations including known SOEC constants. The resulting equations are extensive.

Table 2. Elastic stiffness constants C_{IJ} of 18R martensite Cu–Zn–Al in the orthorhombic approximation at room temperature. The units are GPa.

C_{11}	C_{22}	C_{33}	C_{44}	C_{55}	C_{66}	C_{12}	C_{13}	C_{23}	Ref.
176 ± 1	158 ± 8	232 ± 2	53 ± 2	26 ± 1	48 ± 2	112 ± 10	37 ± 10	150 ± 15	This work
178 ± 4	152 ± 12	237 ± 1	55 ± 4	27 ± 1	48 ± 12	108 ± 21	41 ± 32	154 ± 31	[13]
175 ± 4	156 ± 1	235 ± 4	54 ± 1	28 ± 2	48 ± 1	118 ± 4	40 ± 20	150 ± 30	[12]

the number of C_{IJ} has allowed us to minimize the intrinsic error associated with the experimental measurement of the ultrasonic wave velocity. Determination of the complete set of results required substantial algebraic and numerical manipulation of the expressions given in table 1. To expedite this task, the scientific software *Mathematica*™ was employed. Details need not be reported here. The resulting second-order elastic stiffness tensor components C_{IJ} at room temperature are compared with those reported elsewhere in table 2; the room-temperature density has been taken as 7589 kg m^{-3} [12]. Since these data sets were obtained using different experimental approaches, the agreement between them is reasonable. Table 3 shows the expressions for the elastic compliance constants S_{IJ} and the bulk modulus for an orthorhombic crystal as a function of the elastic stiffness tensor components together with the numerical values corresponding to the samples examined here.

To study the effects of pressure on the elastic behaviour of the alloy, the pressure dependence $[\partial f/\partial P]_{P=0}$ of the pulse echo overlap frequency f was measured for 15 propagation ultrasonic modes at room temperature. The overlap frequency change increased linearly with increasing pressure. For each measurement, data points were taken

Table 3. Expressions for the elastic compliance constants S_{IJ} and the bulk modulus for an orthorhombic crystal as a function of the SOEC. The values of S_{IJ} (in units of $10^{-11}\mathrm{N}^{-1}\mathrm{m}^2$) and bulk modulus (in GPa) are given for 18R martensite Cu–Zn–Al at room temperature.

$S_{11} = \frac{-C_{23}^2+C_{22}C_{33}}{A}$ $S_{22} = \frac{-C_{13}^2+C_{11}C_{33}}{A}$ $S_{44} = \frac{1}{C_{44}}$

$S_{12} = \frac{C_{13}C_{23}-C_{12}C_{33}}{A}$ $S_{22} = \frac{C_{12}C_{13}-C_{11}C_{23}}{A}$ $S_{55} = \frac{1}{C_{55}}$

$S_{13} = \frac{-C_{13}C_{22}+C_{12}C_{23}}{A}$ $S_{33} = \frac{-C_{12}^2+C_{11}C_{22}}{A}$ $S_{66} = \frac{1}{C_{66}}$

$$B = \frac{C_{11}C_{22}C_{33}+2C_{12}C_{13}C_{23}-C_{11}C_{23}^2-C_{12}^2C_{33}-C_{13}^2C_{22}}{C_{11}(C_{22}+C_{33}-2C_{23})+2C_{12}(C_{13}+C_{23}-C_{33})+2C_{13}(C_{23}-C_{22})+C_{22}C_{33}-C_{12}^2-C_{13}^2-C_{23}^2}$$

$$A = C_{11}C_{22}C_{33} + 2C_{12}C_{13}C_{23} - C_{11}C_{23}^2 - C_{12}^2C_{33} - C_{13}^2C_{22}$$

S_{11}	S_{22}	S_{33}	S_{44}	S_{55}	S_{66}	S_{12}	S_{13}	S_{23}	B	Ref.
2.33	6.49	2.51	1.89	3.85	2.08	−3.36	1.80	−3.66	112	This work
2.30	7.57	2.88	1.82	3.70	2.08	−3.60	1.94	−4.30	120	[13]
3.80	10.62	3.59	1.85	3.57	2.08	−5.84	3.08	−5.78	108	[12]

during both increasing and decreasing pressure runs; there was no observable hysteresis effect under pressure cycling. Values given in table 1 for $[\partial f/\partial P]_{P=0}$ correspond to averaged data for several runs, and the error is the maximum deviation from the mean value.

The pressure derivatives of ρV^2 to the basic frequency data and coefficients at zero pressure are related by [19]

$$\left[\frac{\partial(\rho V^2)}{\partial P}\right]_{P=0} = \rho V_0^2\left[\frac{2(\partial f/\partial P)_{P=0}}{f_0} + \frac{1}{B_0} - 2N_kN_mS_{kmii}^T\right]. \tag{2}$$

Here ρ, B_0 and V_0 are the density, bulk modulus and ultrasonic mode velocity respectively at ambient conditions. In addition N_i are the components of the propagation vector and S_{ijkl}^T the components of the isothermal elastic compliance tensor. The last two terms in the bracket on the right-hand side of equation (2) correspond to the effects of changes of density and path length, respectively. In this work the isothermal S_{ijkl}^T $(=S_{ijkl}^S+\alpha_{ij}\alpha_{kl}T/C_p)$ have been replaced by the adiabatic elastic compliances because there have been as yet no measurements of the volume thermal expansion tensor α_{ij}. However, the error introduced by assuming $S_{ijkl}^T \approx S_{ijkl}^S$ is negligible compared with other experimental errors. The effect of hydrostatic pressure on the ultrasonic wave velocities is shown in figure 1 for each of the modes with propagation and polarization directions listed in table 1. The measured relative change in the velocity of the ultrasonic modes, computed by fitting a straight line to the measured dependence, is also given in table 1. Numerical treatment of the data for $[\partial(\rho V^2)/\partial P]_{P=0}$ provided the complete set of the pressure derivatives $(\partial C_{IJ}/\partial P)_{P=0}$ for all the elastic stiffness tensor components. For every acoustic mode examined, ultrasonic wave velocity increases with pressure; this would be expected for normal anharmonic behaviour of the long-wavelength acoustic modes. Hence the pressure derivatives of the elastic stiffness constants are positive (table 4).

To calculate the mode Grüneisen parameters, it is helpful to know the values of the pressure derivatives of the second-order thermodynamic elastic constants B_{IJ}, which are also called thermodynamic coefficients. The values of $\partial C_{IJ}/\partial P$, that have actually been obtained (table 4), correspond to the pressure derivatives of the effective stiffness tensor components; these differ from the thermodynamic coefficients,

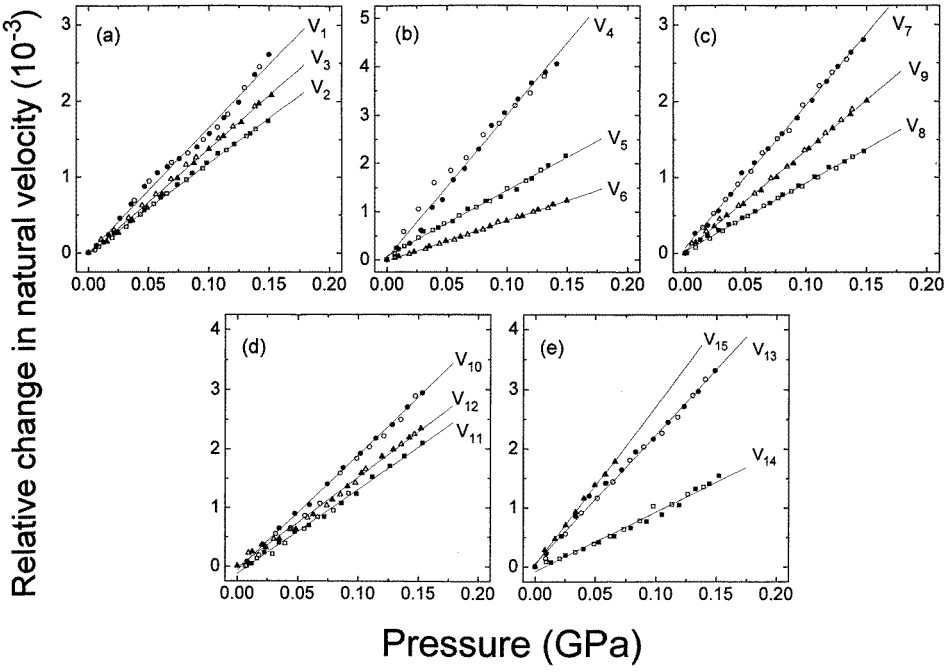

Figure 1. The relative change with hydrostatic pressure in natural velocity of ultrasonic waves propagated in Cu–Zn–Al 18R martensite at 293 K. Curves are labelled according to table 1. For each propagation direction: (a) $\boldsymbol{N} = [001]$; (b) $\boldsymbol{N} = [010]$; (c) $\boldsymbol{N} = [100]$; (d) $\boldsymbol{N} = [3\bar{2}0]$; (e) $\boldsymbol{N} = [\bar{1}\bar{2}8]$ we obtain longitudinal (circle), fast shear (square) and slow shear modes (triangle). Full and empty symbols corresponds to increasing and decreasing pressure runs respectively, and solid lines are linear fits to the data.

Table 4. The effective pressure derivatives $(\partial C_{IJ}/\partial P)_{P=0}$ and the pressure derivatives B_{IJ} of the thermodynamic SOEC of 18R martensite Cu–Zn–Al at room temperature.

$(\partial C_{IJ}/\partial P)_{P=0}$		B_{IJ}	
$\partial C_{11}/\partial P$	5.25 ± 0.12	B_{11}	10.1
$\partial C_{22}/\partial P$	11.9 ± 0.4	B_{22}	8.15
$\partial C_{33}/\partial P$	7.12 ± 0.40	B_{33}	12.1
$\partial C_{44}/\partial P$	1.01 ± 0.05	B_{44}	1.66
$\partial C_{55}/\partial P$	0.57 ± 0.04	B_{55}	2.08
$\partial C_{66}/\partial P$	0.53 ± 0.03	B_{66}	1.33
$\partial C_{12}/\partial P$	9.04 ± 0.91	B_{12}	7.58
$\partial C_{13}/\partial P$	11.5 ± 1.4	B_{13}	11.3
$\partial C_{23}/\partial P$	16.7 ± 6.1	B_{23}	14.8

which are defined in terms of the second derivatives with respect to strain of the internal energy, when the strain is referred to the natural 'zero'-pressure state [19]. In fact, at atmospheric pressure the effective elastic stiffness tensor components approach quite closely the values of the thermodynamic ones; in some cases the pressure derivatives of the two sets of coefficients can differ considerably from each other. For an orthorhombic crystal relations between $\partial C_{IJ}/\partial P$ and B_{IJ} are given by

[20]

$$
\begin{aligned}
B_{11} &= \frac{\partial C_{11}}{\partial P} + 1 - (S_2 + S_3 - 3S_1)C_{11} \\
B_{33} &= \frac{\partial C_{33}}{\partial P} + 1 - (S_1 + S_2 - 3S_3)C_{33} \\
B_{12} &= \frac{\partial C_{12}}{\partial P} - 1 - (S_3 - S_1 - S_2)C_{12} \\
B_{44} &= \frac{\partial C_{44}}{\partial P} + 1 - (S_1 - S_2 - S_3)C_{44} \\
B_{13} &= \frac{\partial C_{13}}{\partial P} - 1 - (S_2 - S_1 - S_3)C_{13} \\
B_{55} &= \frac{\partial C_{55}}{\partial P} + 1 - (S_2 - S_1 - S_3)C_{55} \\
B_{22} &= \frac{\partial C_{22}}{\partial P} + 1 - (S_3 + S_1 - 3S_2)C_{22} \\
B_{66} &= \frac{\partial C_{66}}{\partial P} + 1 - (S_3 - S_1 - S_2)C_{66} \\
B_{23} &= \frac{\partial C_{23}}{\partial P} - 1 - (S_1 - S_2 - S_3)C_{23}
\end{aligned}
\tag{3}
$$

where $S_1 = S_{11} + S_{12} + S_{13}$, $S_2 = S_{12} + S_{22} + S_{23}$ and $S_3 = S_{13} + S_{23} + S_{33}$; the numerical values obtained are tabulated in table 4.

3.2. Acoustic mode vibrational anharmonicity and Grüneisen parameters

The pressure variations of the elastic stiffness tensor components, which have been measured, determine the lowest-order term for the acoustic-mode anharmonicity, and hence the non-linearity of interatomic forces with respect to atomic displacements. It is customary to discuss the anharmonic properties in terms of generalized Grüneisen parameters $\gamma_p(\boldsymbol{N})$. These parameters quantify to first order the volume or strain dependence of the lattice vibrational frequencies $\omega_p(\boldsymbol{q})$ of the acoustic modes at the Brillouin zone centre induced by hydrostatic pressure-induced changes in the lattice potential. In the elastic continuum model at the long-wavelength limit, a general relationship expresses the acoustic-mode Grüneisen parameters $\gamma_p(\boldsymbol{N})$, where p denotes the branch and $\boldsymbol{N}$ is a unit vector in the propagation direction, in terms of second- and third-order elastic constants (C_{ijklmn}) [21]

$$
\gamma_p(\boldsymbol{N}) = -\frac{1}{2\omega_p(\boldsymbol{N})\chi^T}[1 + S^T_{aajk}(2\omega_p(\boldsymbol{N})U_jU_k + C_{jkmunv}N_mN_nU_uU_v)]. \tag{4}
$$

Here $\boldsymbol{U}$ is a unit vector along the polarization direction appropriate to the index p, and χ^T is the isothermal compressibility. Since these mode Grüneisen parameters relate only to hydrostatic pressure, they can be determined from the elastic constants and their hydrostatic pressure derivatives alone; for this purpose it is not necessary to consider contributions to the third-order constants induced by application of uniaxial stress. Determination of the mode Grüneisen parameters can be achieved by means of the thermodynamic coefficients B_{IJ} (equation (3)). Thurston [19] provides the useful relationship

$$
B_{IJ} = -(S_1C_{IJ1} + S_2C_{IJ2} + S_3C_{IJ3}). \tag{5}
$$

Combination of the third-order elastic constants and the second-order elastic compliances in the mode Grüneisen equation (4) leads to expressions for the Grüneisen parameters that depend only upon the thermodynamic coefficients B_{IJ}. Expressions have been developed here which apply specifically to orthorhombic crystals:

$$\begin{aligned}{}_H\gamma_p^T(\boldsymbol{N}) = -\frac{1}{2w\chi^T}\{1 + 2w[&(S_{11}^T + S_{12}^T + S_{13}^T)U_1^2 + (S_{12}^T + S_{22}^T + S_{23}^T)U_2^2 \\ &+(S_{13}^T + S_{23}^T + S_{33}^T)U_3^2] - B_{11}N_1^2U_1^2 - B_{22}N_2^2U_2^2 - B_{33}N_3^2U_3^2 \\ &-2B_{12}N_1N_2U_1U_2 - 2B_{13}N_1N_3U_1U_3 - 2B_{23}N_2N_3U_2U_3 \\ &-B_{44}(N_2U_3 + N_3U_2)^2 - B_{55}(N_1U_3 + N_3U_1)^2 - B_{66}(N_1U_2 + N_2U_1)^2\} \end{aligned} \tag{6}$$

where

$$\begin{aligned} w = {} & C_{11}N_1^2U_1^2 + C_{22}N_2^2U_2^2 + C_{33}N_3^2U_3^2 + C_{44}(N_2U_3 + N_3U_2)^2 \\ & +C_{55}(N_1U_3 + N_3U_1)^2 + C_{66}(N_1U_2 + N_2U_1)^2 + 2C_{12}N_1N_2U_1U_2 \\ & +2C_{13}N_1N_3U_1U_3 + 2C_{23}N_2N_3U_2U_3 \end{aligned}$$

and

$$\chi^T = S_{11}^T + S_{22}^T + S_{33}^T + 2(S_{12}^T + S_{13}^T + S_{23}^T).$$

By using the values of B_{IJ}, given in table 4, the acoustic-mode Grüneisen parameters in the long-wavelength limit have been calculated for the $Cu_{0.696}Zn_{0.128}Al_{0.176}$ alloy crystal. To do this, the Christoffel equations have been solved to find the mode velocities (as the eigenvalues) and thus the elastic stiffness for each propagation direction, defined by $\boldsymbol{N}$; the polarization directions $\boldsymbol{U}$ have been obtained as the eigenvectors. Results are plotted as a function of mode propagation direction in figure 2. Usually the elastic constants and lattice vibrational frequencies increase with pressure, so that the mode Grüneisen parameters are positive. For the $Cu_{0.696}Zn_{0.128}Al_{0.176}$ alloy, although the longitudinal modes show normal behaviour with the Grüneisen parameter having positive values, the shear modes show the instructive feature of being negative for many propagation directions. It is especially relevant to the transition mechanism that there is a marked dip in a direction close to the $(111)[1\bar{2}1]$ mode because unusual behaviour for this mode has previously been reported [13]. In particular, it has been found that the velocity of elastic waves has a pronounced minimum for a wave propagated along the [111] direction with $[1\bar{2}1]$ polarization vector. Even more interesting is the observation that this mode suffers a relatively large temperature decrease (softening) on approaching the transition. These results suggest that the lattice stability against this particular shear mode decreases as the sample approaches the MT. During the transition the parent phase transforms to the martensite structure by means of a diffusionless transformation. The lattice distortion suffered by the structure in order to reach the low-temperature phase is basically described by a shear. The deformation can be described using a matrix that relates the lattice vectors and planes in both phases [22]. It should be noticed that the shear on the [111] plane and directed along the $[1\bar{2}1]$ direction in the martensite phase is obtained from the $(110)[1\bar{1}0]$ shear in the β-phase using the matrix correspondence between phases. As indicated, this shear is responsible for the main lattice distortion associated with the transition due to the low value of the elastic modulus C'. The mode also exhibits a partial softening with decreasing temperature near M_s. In addition, as shown in the inset of figure 2, the acoustic mode Grüneisen parameter exhibits a marked change (a maximum) for the $(110)[1\bar{1}0]$ mode in the β-phase. It has been found here that the anharmonicity of this mode increases near the transition point. As a result, with changing temperature a considerable variation of the Grüneisen parameter for the slow shear mode

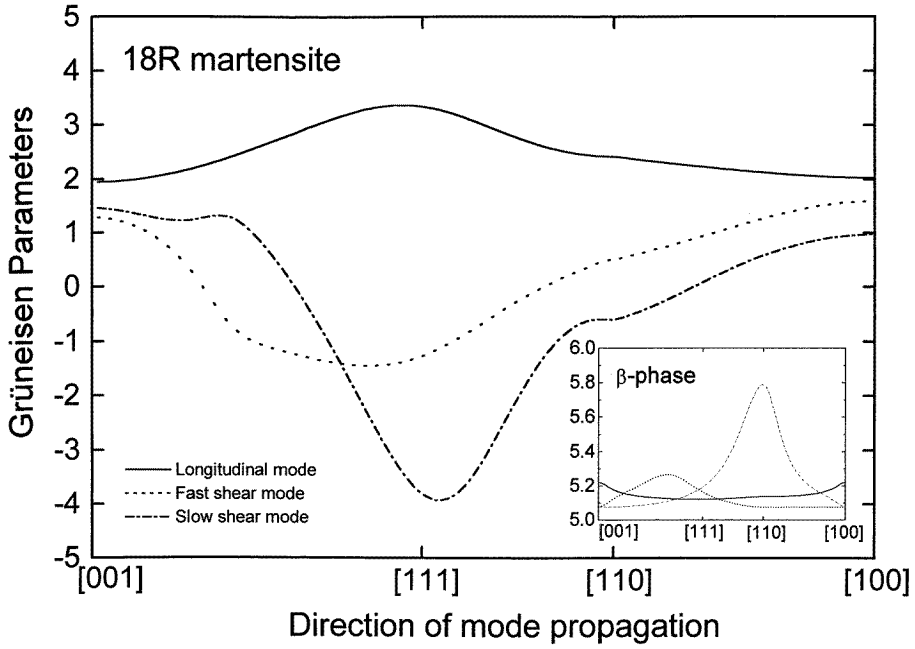

Figure 2. Long-wavelength longitudinal (solid line) and shear (dashed and dotted lines) acoustic-mode Grüneisen parameter of Cu–Zn–Al in the 18R martensite phase and in the β-phase (inset), as a function of mode propagation direction at 293 K. Data for the β-phase were obtained from [8] for $Cu_{0.677}Zn_{0.194}Al_{0.129}$ ($M_s = 280$ K).

propagating in the [111] direction of the martensitic phase occurs. For the bcc Cu–Zn–Al, the soft shear modes associated with C' are much more anharmonic than the remaining modes. In the differing theoretical approaches [5, 23] to the martensitic transition, this anharmonicity has been recognized as being crucial in the mechanisms driving the system towards the transition. The results presented here show that the martensitic structure inherits some degree of this large anharmonicity. In this sense, the minimum in the slow shear branch has to be related to the dynamical instability of the close-packed phase towards the ensuing martensitic transition.

4. Conclusions

(1) The ultrasonic wave velocity for each of the 15 acoustic modes propagated in monocrystalline $Cu_{0.696}Zn_{0.128}Al_{0.176}$ alloy increases linearly with increasing pressure. No measurable hysteresis effects have been observed under pressure cycling up to 0.15 GPa.

(2) The results obtained for the C_{IJ} at ambient pressure, when the structure is treated as being 18R, are in good agreement with previous data obtained using other ultrasonic techniques.

(3) The hydrostatic-pressure derivatives $(\partial C_{IJ}/\partial P)_{P=0}$ of elastic stiffness tensor components have positive values: application of pressure does not induce acoustic-mode softening.

(4) An expression has been derived which gives the acoustic-mode Grüneisen parameters of crystals with orthorhombic symmetry. This expression has been used to calculate the Grüneisen parameters of monocrystalline $Cu_{0.696}Zn_{0.128}Al_{0.176}$ alloy in the 18R structure.

(5) The longitudinal mode Grüneisen parameters have positive values indicating a normal non-linear acoustic behaviour.

(6) Some of the shear modes show unusual behaviour in having negative Grüneisen parameters. A marked dip has been observed in the shear mode Grüneisen parameter for the ultrasonic wave propagated along the [111] direction with $[1\bar{2}1]$ polarization vector. A comparison made with the Grüneisen parameters obtained for the β-phase suggests that the lattice instability against this particular shear mode increases as the sample approaches the martensitic transition.

Acknowledgments

AG and LlM acknowledge CICyT (Spain) for financial support, project No MAT95-0504. We are grateful to NATO (Scientific and Environmental Affairs Division, grant number CRG960584) for financial support. We would like to thank E F Lambson, R C J Draper and W Lambson for technical assistance.

References

[1] Delaey L 1991 *Phase Transformations in Materials, (Materials Science and Technology 5)* ed P Haasen (Weinheim: VCH) p 339
[2] Delaey L, Krishman R V, Tass H and Warlimont H 1974 *J. Mater. Sci.* **9** 1521
Delaey L, Krishman R V, Tass H and Warlimont H 1974 *J. Mater. Sci.* **9** 1536
Delaey L, Krishman R V, Tass H and Warlimont H 1974 *J. Mater. Sci.* **9** 1595
[3] Petry W 1995 *J. Physique Coll.* **5** C2 15
[4] Lindgård P A and Mouritsen O G 1986 *Phys. Rev. Lett.* **57** 2458
[5] Morris J R and Gooding R J 1990 *Phys. Rev. Lett.* **65** 1769
[6] Nishiyama Z and Kajiwara S 1963 *Japan. J. Appl. Phys.* **2** 478
[7] Lovey F C 1987 *Acta Metall.* **35** 1103
[8] Verlinden B, Suzuki T, Delaey L and Guénin G 1984 *Scr. Metall.* **18** 975
[9] Gonzàlez-Comas A and Mañosa Ll 1996 *Phys. Rev.* B **54** 6007
[10] Nagasawa A, Kuwabara A, Morii Y, Fuchizaki K and Funahashi S 1992 *Mater. Trans. JIM* **33** 203
[11] Jurado M, Cankurtaran M, Mañosa Ll and Saunders G A 1992 *Phys. Rev.* B **46** 14 174
[12] Rodríguez P L, Lovey F C, Guénin G, Pelegrina J L, Sade M and Morin M 1993 *Acta Metall. Mater.* **41** 3307
[13] Gonzàlez-Comas A, Mañosa Ll, Planes A, Lovey F C, Pelegrina J L and Guénin G 1997 *Phys. Rev.* B **56** 5200
[14] Papadakis E P 1967 *J. Acoust. Soc. Am.* **42** 1045
[15] Thurston R N and Brugger K 1964 *Phys. Rev.* **133** A1604
[16] Flower S C and Saunders G A 1990 *Phil. Mag.* B **62** 311
[17] Nye J F 1987 *Physical Properties of Crystals* (Oxford: Oxford University Press) p 140
[18] Shutilov V A 1988 *Fundamental Physics of Ultrasound* (Amsterdam: Gordon and Breach) p 304
[19] Thurston R N 1965 *Proc. IEEE* **53** 1320
[20] Thurston R N 1965 *J. Acoust. Soc. Am.* **37** 348
[21] Brugger K 1965 *Phys. Rev.* **137** A1826
[22] Kajiwara S 1986 *Mater. Trans. JIM* **17** 435
[23] Kerr W C, Hawthorne A M, Gooding R J, Bishop A R and Krumhansl J A 1992 *Phys. Rev.* B **45** 7036